Dalton Transactions

PAPER

View Article Online
View Journal

Cite this: DOI: 10.1039/c5dt04288g

Preorganized tridentate analogues of mixed hydroxyoxime/carboxylate nickel extractants†

James W. Roebuck,[a] Jennifer R. Turkington,[a] David M. Rogers,[a] Philip J. Bailey,[a] Violina Griffin,[b] Adam J. Fischmann,[b] Gary S. Nichol,[a] Max Pelser,[c] Simon Parsons[a] and Peter A. Tasker*[a]

A series of 22 tridentate unsaturated mono-anionic ligands having the atom-sequence Y–C═C–N═CH–C═C–Z^{-1}, with Y = N, O, or S and Z = O or S, has been studied to establish whether this backbone could be used to develop strong solvent extractants for nickel(II) which will preferably also show a high selectivity over iron(III) in the pH-dependent process: $2LH_{org} + NiSO_4 \rightleftharpoons [(L)_2Ni]_{org} + H_2SO_4$. All are capable of forming octahedral $[(L)_2Ni]$ complexes with a *mer*-arrangement of the YNZ^{-1} donor set. X-ray crystal structures of three salicylaldimine proligands derived from 3-bromo-5-*t*-butyl-2-hydroxybenzaldehyde show these to have pre-organised donor sets in which the three donors are held in an approximately orthogonal arrangement by intramolecular hydrogen bonds. The tautomers observed are dependent on the nature of the Y atom and the extent to which it is favourable for this to form a bonding interaction with the acidic hydrogen atom on the salicylaldimine unit. X-ray crystal structure determinations of seven of the $[(L)_2Ni]$ complexes show these to have significantly distorted octahedral coordination geometries which partly account for the proligands proving to be fairly weak Ni-extractants. DFT calculations show that extractant strength is dependent on a combination of the binding strength of the YNZ^{-1} donor set to the nickel ion and on the ease of deprotonation of the extractant. On this basis 3-nitro-4-*t*-octyl-6-(quinolin-8-imino)phenol is predicted, and is found, to be the strongest Ni-extractant. The extractants have low hydrolytic stability, reverting to their aldehyde precursors when solutions in water-immiscible solvents are contacted with aqueous acid, making them poor candidates for development as reagents for nickel recovery based on pH-swing processes of the type shown above.

Received 31st October 2015,
Accepted 11th January 2016

DOI: 10.1039/c5dt04288g

www.rsc.org/dalton

Introduction

The increasing demand for nickel arising from its expanding uses in stainless steel, electroplating and rechargeable batteries[1] is providing an incentive for the mining industry to develop more efficient processes for its recovery from laterite ores as a consequence of the declining grade and the dearth of discoveries of sulfidic ores,[2] which are processed using conventional pyrometallurgy.[3] Low grade nickelferrous laterite ores, which contain high concentrations of water and iron, are more abundant and can be processed by hydrometallurgical methods following High Pressure Acid Leaching (HPAL),[4] but downstream recovery of metals is inefficient and is currently preceded by raising the pH to precipitate iron(III) oxyhydroxide waste.[5] The ARFe (Anglo Research Iron) process[2,6] generates hematite as a product of commercial value and provides options for recovery of cobalt and nickel from acidic sulfate streams. This paper considers how new solvent extractants might be designed to concentrate and separate nickel from such streams, using the pH-dependent equilibrium shown in eqn (1).

$$M^{2+} + 2LH_{org} \rightleftharpoons [L_2M]_{org} + 2H^+ \quad (1)$$

Cyanex® 301, a dialkyldithiophosphinic acid, has been shown to be effective for the direct recovery of nickel and cobalt without pH adjustment.[7] Due to reduced stability in the presence of oxidizing agents, Cyanex 301 must be used under an inert atmosphere in a closed system, achieved at Goro with the use of very large pulsed columns.[8,9] The multi-branched decanoic acid, Versatic® 10, has been tested extensively for nickel recovery from laterite streams but is a weak extractant,[10] requiring several contacts with pH-adjustment to displace the

[a]EaStCHEM School of Chemistry, University of Edinburgh, David Brewster Road, Edinburgh, Scotland EH9 3FJ, UK. E-mail: p.a.tasker@ed.ac.uk
[b]Cytec Industries, 1937 West Main Street, Stamford, Connecticut 06902, USA
[c]Anglo American, 8 Schonland Street, Theta, Johannesburg, 2091, South Africa

† Electronic supplementary information (ESI) available. CCDC 1433304, 1410169, 1410168, 1448162, 1433302, 1433538, 1410171, 1430069, 1433306 and 1430068. For ESI and crystallographic data in CIF or other electronic format see DOI: 10.1039/c5dt04288g

equilibrium shown in eqn (1).‡ It also has a high solubility in aqueous streams, requiring an additional extractant-recovery step.[11] The use of synergistic combinations of an organic acid and a neutral extractant has been shown to enhance the efficiency of nickel recovery greatly, but so far none of these have been implemented in commercial operations.[12] One of the best understood synergistic systems contains a mixture of a carboxylic acid such as Versatic® 10 and an α-hydroxyoxime, such as LIX® 63 (see Fig. 1).[13,14] The extraction equilibrium is thought to involve the deprotonation of the carboxylic acid, rather than the hydroxyoxime as in eqn (2).

$$Ni^{2+} + 2RCOOH_{org} + 2ox_{org} \rightleftharpoons [Ni(RCOO\cdot ox)_2]_{org} + 2H^+ \quad (2)$$

An X-ray structure of the model system shown in Fig. 1b,[13] contains a pseudooctahedral, charge-neutral, nickel complex with two carboxylate and two neutral hydroxyoxime ligands. Hydrogen bonding between the ligands generates a planar pseudo-tridentate $[NO_2]^-$ donor set which forms a sequence of 5/7-membered chelate rings (Fig. 1c). The N–OH group of the oxime unit acts as a hydrogen bond donor to the carboxylate rather than the α-hydroxy (C–OH) group which would give the 5/6-membered chelate ring sequence shown in Fig. 1d.

This paper considers whether single hydrophobic ligand molecules with comparable tridentate donor sets can generate sufficiently stable and soluble complexes to extract nickel from more acidic solutions than the LIX 63/Versatic system. The salicylaldimines, **L1H–L19H**, and the acylpyrazolone- and acylthiopyrazolone-imines **L20H–L22H** shown in Fig. 2 were selected for testing as these should all be readily deprotonated to give bis *mer*-Ni^{2+}-complexes with approximately planar YNZ^- donor sets favoured by the conjugation in the ligands (Fig. 3). If extractants of this type were to be used to recover nickel efficiently from laterite leach streams it would be very beneficial if they were able to transport nickel selectively into the organic phase, rejecting iron, because this would remove the need for precipitation of the latter. In the presence of iron(III) extractants should give cationic $[FeL_2]^+$ complexes, of the type characterised by Brashoveanu *et al.*,[15] that will require a counterion to balance the charge on the complex. Such salts are likely to have low solubility in the hydrocarbon diluents used in solvent extraction and this will result in preferential recovery of nickel(II) over iron(III).

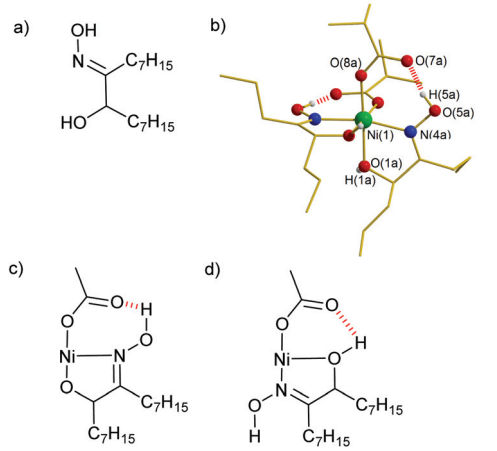

Fig. 1 The structure of LIX63 (a); the X-ray crystal structure of [Ni(^{n}Pr–hydroxyoxime)$_2$(^{i}Pr–CO$_2$)$_2$] (b);[13] the 7/5 membered ring H-bonding arrangement observed in [Ni(^{n}Pr–hydroxyoxime)$_2$(^{i}Pr–CO$_2$)$_2$] (c); and the alternative 5/6 membered ring arrangement (d).

‡Metal extraction by hydrophobic carboxylic acids often involves more complicated stoichiometries than those implied in eqn (1). When the extractant is present in excess, usually both carboxylate anions and neutral carboxylic acid molecules are coordinated to the metal ion. These arrangements allow the hydrogen bonds, which are favoured in the metal free extractant, to be retained in the supramolecular configuration of the extracted.[11]

Results and discussion

Synthesis and characterization of the proligands

Three 3-substituted-5-*tert*-butyl-salicylaldyde precursors[16] (2–4; for structures see ESI†) for **L1H–L3H**, **L8H–L10H** and **L12H–L14H** were condensed with 8-aminoquinoline or with 2-methoxyaniline or 2-thiomethoxyaniline to yield the proligands. Two 3-substituted-5-*tert*-octyl-salicylaldyde precursors[16] (**5** and **6**) were used to prepare **L4H**, **L5H**, **L11H** and **L15H** in an attempt to enhance the solubility of the extractants and their

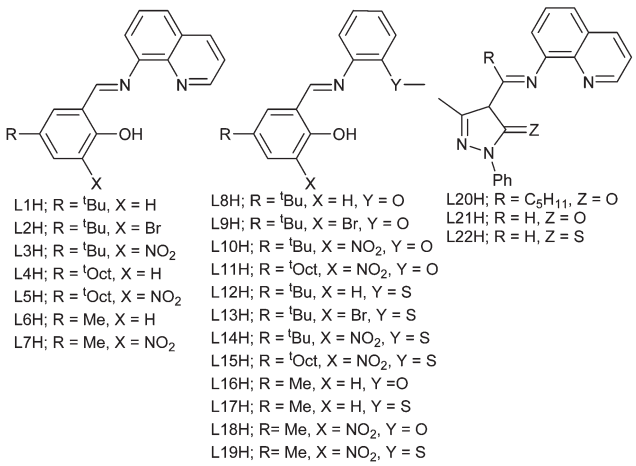

Fig. 2 Tridentate salicylaldimine (**L1H–L19H**), acylpyrazoloneimine (**L20H** and **L21H**) and acyl thiopyrazoloneimine (**L22H**) proligands.

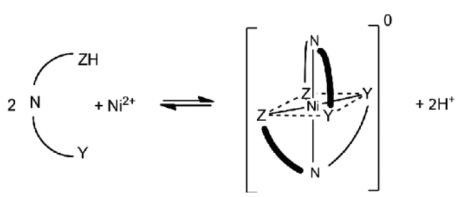

Fig. 3 The formation of a neutral octahedral nickel(II) complex by *mer*-forms of the monoanionic tridentate ligands formed by deprotonation of **L1H–L22H**.

nickel(II) complex. The acylpyrazolone imines **L20H** and **L21H** were obtained from similar Schiff base condensations using 1-phenyl-3-methyl-5-oxo-4,5-dihydro-1*H*-pyrazole-4-carbaldehyde (**1**) or 4-hexanoyl-3-methyl-1-phenyl-4,5-dihydro-1*H*-pyrazol-5-one (**7**). **L22H** was obtained by the two step, one pot, reaction of 1-(5-chloro-3-methyl-1-phenyl-4,5-dihydro-1*H*-pyrazol-4-yl) ethan-1-one shown in Scheme 1 using conditions developed by Smith *et al.*[17]

Proligand structures

The conjugation through the imine moiety and intramolecular hydrogen bonding in the salicylaldimine (Fig. 4a) and the acylpyrazoloneimine proligands (Fig. 4b) was expected to favour the pre-organisation of the donor atoms to generate a planar 6/5 chelate sequence. The extent to which the resulting donor set is orthogonal is important if the ligands are to define a regular octahedral geometry about a nickel(II) ion.

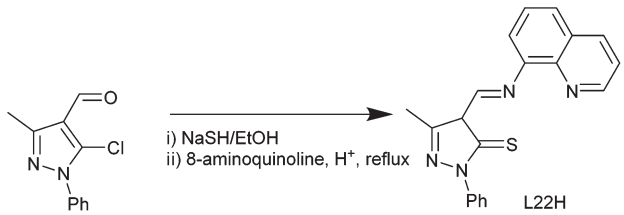

Scheme 1 The one-pot synthesis of **L22H**.

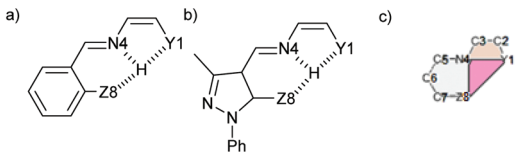

Fig. 4 Salicylaldimine and acylpyrazolone imine proligand structures (a and b) with approximately orthogonal Z8, N4 and Y1 donor atoms, using the atom labelling in X-ray structure determinations below and (c) the Y1–N4–Z8 plane, and the Y1–C2–C3–N4 and N4–C5–C6–C7–Z8 least squares planes used in structure analysis (Table 1).

Data presented in Table 1 define the geometries of the pre-organised donor atoms in the crystal structures of **L2H**, **L9H** and **L13H**. The structure of **L9H** has three crystallographically independent molecules per asymmetric unit (Fig. 5). Molecule **b** is the most nearly planar with the linking carbon atoms showing ≤0.04 Å deviations from the plane defined by the Y1–N4–Z8 donor set of the proligand. Molecules **a** and **c** are less planar with larger (maximum) deviations of the linking carbon atoms from the Y1–N4–Z8 plane of 0.85 and 0.65 Å respectively, and have similar conformations with the five- and six-membered potential chelating units being displaced to opposite sides of the Y1–N4–Z8 plane. The phenolic imine N4–C5–C6–C7–Z8 units show a larger inclination from this plane (25 and 40° in molecules **a** and **c**) than the methoxy imine N4–C3–C2–Y1 units for which the least squares planes are inclined by 16 and 27°. A difference map calculated during the solution of the structure of **L9H** indicated that the acidic hydrogen atom in molecule **b** is disordered between the phenolic oxygen, O(8b), and the imine nitrogen, N(4b), and refinement showed a 7 : 3 occupancy of these sites which correspond to the tautomers shown at the bottom of Fig. 5. The solid state structures of **L2H** and **L13H** both contain two crystallographically independent molecules per unit cell. Only molecules **a** are shown in Fig. 6. Inter-molecular contact distances are listed in Table 2. The thioether-substituted proligand, **L13H**, exists exclusively as the conventional phenolic imine whereas **L2H** has the acidic hydrogen atom attached to N4 where it can form comparably strong hydrogen bonds to the quinone oxygen and quinoline nitrogen atoms, with contact distances of 2.6 and 2.7 Å respectively. This bifurcated hydrogen bonding relationship favours a highly planar conformation of the proligand.

Table 1 A comparison of the geometries of the Br-substituted salicylaldimine proligands, **L2H**, **L9H** and **L13H**

Ligand	**L2H** (Y=N, Z=O)		**L9H** (Y=O, Z=O)			**L13H** (Y=S, Z=O)	
Molecule	**a**	**b**	**a**	**b**	**c**	**a**	**b**
Angles/° between donor atoms and Z8–Y1 midpoint (H)[a]							
Y1–M–N8	91.84	92.12	91.36	91.12	91.36	95.16	95.86
Z8–M–N4	88.16	87.88	88.64	88.88	88.64	84.39	84.14
Y1–N4–Z8	84.70	83.30	95.34	79.79	95.84	77.61	78.17
Angle/° between the Z, N8, Y and the N8, C7, C6, C1, Z least squares planes[a]							
γ	10.37(5)	9.51(8)	25.07(7)	0.96(8)	39.89(8)	13.08(2)	13.93(2)
Angle/° between the Z, N8, Y and N8, C9, C14, Y least squares planes[a]							
δ	3.57(6)	3.68(8)	15.85(9)	0.04(1)	26.62(1)	4.97(2)	2.64(2)
Displacement/Å from the Z, N8, Y least squares plane[a]							
C7	0.255(1)	0.198(1)	0.600(2)	−0.003(1)	−0.658(2)	0.294(3)	0.358(3)
C6	0.357(1)	0.335(1)	0.858(2)	0.571(2)	−0.880(2)	0.451(3)	0.479(3)
C5	0.220(1)	0.218(1)	0.511(2)	0.326(2)	−0.470(2)	0.327(3)	0.303(3)
C3	0.052(1)	0.001(2)	−0.328(2)	−0.050(2)	0.443(2)	−0.120(4)	−0.062(3)
C2	0.102(1)	−0.002(2)	−0.350(2)	0.002(2)	0.475(2)	−0.126(4)	−0.068(3)

[a] Atom labelling scheme is provided in Fig. 4.

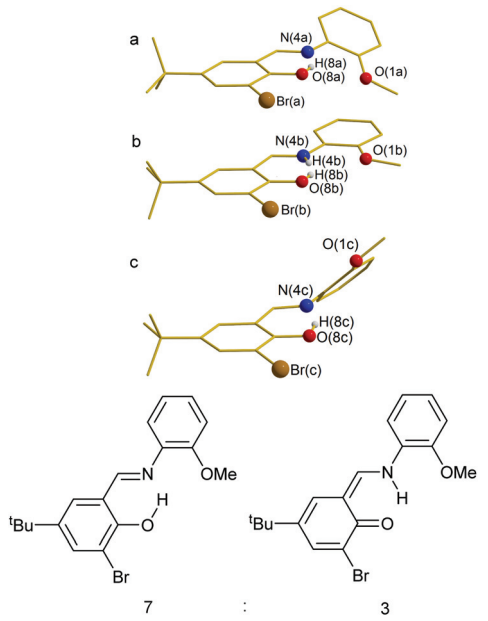

Fig. 5 The structures of the three crystallographically independent molecules of **L9H**, (a–c). The disorder of the acidic protons H(8) and H (4) in the molecule b corresponds to a 7 : 3 occupancy of the phenol/quinone tautomers shown.

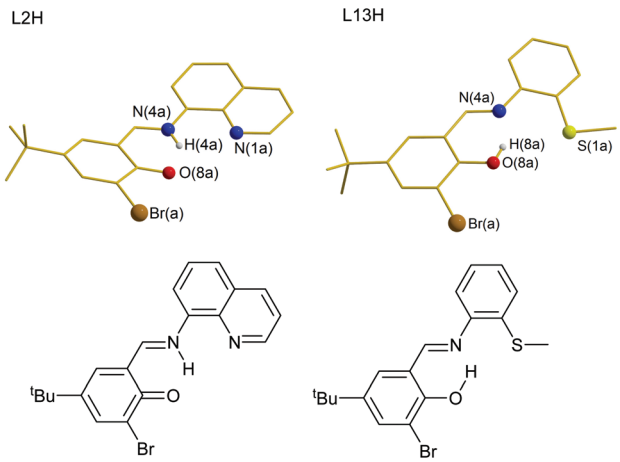

Fig. 6 The X-ray crystal structures of **L2H** and **L13H**.

Table 2 Intra-molecular contact distances for the Br-substituted salicylaldimine proligands, **L2H**, **L9H** and L13

L2H hydrogen bond (D···A) distances/Å			
N(4a)–H(4a)···O(8a)	2.603(1)	N(4b)–H(4b)···O(8b)	2.579(1)
N(4a)–H(4a)···N(1a)	2.688(1)	N(4b)–H(4b)···N(1b)	2.676(1)
L9H hydrogen bond (D···A) distances/Å			
O(8a)–H(8a)···N(4a)	2.579(2)	O(8b)–H(8b)···N(4b)	2.532(2)
O(8b)–H(8b)···O(1b)	3.280(2)	O(8c)–H(8c)···N(4c)	2.567(2)
O(8a)–H(8a)···O(1a)	3.708(2)	O(8c)–H(8c)···O(1c)	3.856(2)
L13H hydrogen bond (D···A) distances/Å			
O(8a)–H(8a)···N(4a)	2.566(4)	O(8a)–H(8a)···S(1a)	3.384(3)
O(8b)–H(8b)···N(4b)	2.575(4)	O(8b)–H(8b)···S(1b)	3.444(3)

The linking carbon atoms show smaller deviations from the Y1–N4–Z8 plane (≤0.35 Å) than in **L9H**. **L13H** shows very weak hydrogen bonding between the phenolic protons and the sulfur atoms of the thioether groups with long contacts (*ca.* 3.4 Å). The crystal structures of the proligands suggest that the quinoline-containing **L2H** has the most nearly planar pre-organised (*mer*) arrangement of donor atoms as judged by the angles and distances listed in Table 1.

Nickel complex structures

The atom labelling scheme for the X-ray crystal structures of $[(\mathbf{L2})_2Ni]$, $[(\mathbf{L3})_2Ni]$, $[(\mathbf{L9})_2Ni]$, $[(\mathbf{L10})_2Ni]$, $[(\mathbf{L13})_2Ni]$, $[(\mathbf{L14})_2Ni]$ and $[(\mathbf{L22})_2Ni]$ is shown in Fig. 4 and 7. All contain two monoanionic ligands with *mer* arrangements of the tridentate $[Y1–N4–Z8]^-$ donor sets, where Z = O or S, and Y = O or N or S. A comparison of the distorted octahedral geometries is provided in Table 3. The salicylaldimine nickel complexes (see for example $[(\mathbf{L2})_2Ni]$ and $[(\mathbf{L9})_2Ni]$ in Fig. 7) have intra-ligand *cis*-angles in the range 75.05 to 83.76° for their 5-membered chelating units and 87.76 to 96.54° for their 6-membered chelates. The *trans*-angles range between 161.02 and 171.30° and the angles (α) between the Y1–N4–Z8 planes vary between 87.47 and 89.21°. Intra-ligand *trans*-angles in the thiopyrazolone complex $[(\mathbf{L22})_2Ni]$ (see Fig. 7) and the pseudo-tridentate complex, $[Ni(^{n}Pr–hydroxyoxime)_2(^{i}Pr–COOH)_2]$ b) in Fig. 1, are closer to 180° (between 176.55 and 177.71°).

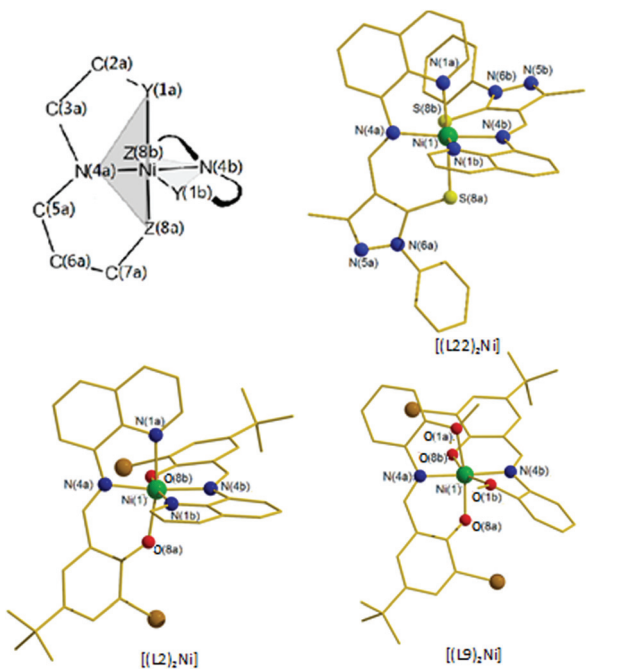

Fig. 7 The atom labelling system for nickel(II) complexes with two monoanionic ligands *a* and *b* coordinating *via* donor atoms Y1, N4 and Z8 which have linking carbon atoms (C2 and C3 and C5, C6 and C7) and the X-ray crystal structures of $[(\mathbf{L22})_2Ni]$ (top right), $[(\mathbf{L2})_2Ni]$ (bottom left) and $[(\mathbf{L9})_2Ni]$ (bottom right).

Table 3 A comparison of the coordination geometries of the salicylyaldimine and pyrazolone imine nickel complexes

Structure	[(**L2**)$_2$Ni] (Y=N, Z=O)				[(**L3**)$_2$Ni] (Y=N, Z=O)		[(**L9**)$_2$Ni] (Y=O, Z=O)	[(**L10**)$_2$Ni] (Y=O, Z=O)		[(**L13**)$_2$Ni] (Y=S, Z=O)		[(**L14**)$_2$Ni] (Y=S, Z=O)		[(**L22**)$_2$Ni] (Y=N, Z=S)		[Ni(^{n}Pr–hydroxyoxime)$_2$-(^{i}Pr–CO$_2$)$_2$][13] (Y=O, Z=O)	
Ligand	**a**	**b**	**a**[b]	**b**[b]	**a**	**b**	**a≡b**[c]	**a**	**b**	**a**	**b**	**a**	**b**	**a**	**b**	**a**	**b**
Bond lengths/Å																	
Ni–Y	2.089(2)	2.114(2)	2.107(2)	2.146(2)	2.091(1)	2.091(1)	2.216(2)	2.181(2)	2.177(2)	2.491(1)	2.412(1)	2.453(1)	2.425(1)	2.091(2)	2.084(2)	2.032(2)	2.026(1)
Ni–N8	2.030(2)	2.040(2)	2.030(2)	2.027(2)	2.038(2)	2.041(2)	2.015(2)	2.004(2)	2.006(3)	2.031(2)	2.041(2)	2.027(2)	2.025(2)	2.080(2)	2.079(2)	2.061(2)	2.057(2)
Ni–Z	2.024(1)	2.047(1)	2.046(1)	2.068(1)	2.054(1)	2.053(1)	1.964(1)	1.988(2)	1.984(2)	2.017(2)	1.988(2)	2.020(3)	1.989(2)	2.385(1)	2.370(2)	2.076(2)	2.083(2)
Interatomic bond angles/°																	
Y–Ni–N8	80.84(7)	80.23(7)	79.97(7)	79.55(7)	80.47(6)	80.49(6)	75.05(7)	77.89(10)	77.89(10)	81.95(7)	83.76(7)	82.90(9)	83.52(6)	80.29(6)	80.72(6)	104.65(7)	103.93(7)
N8–Ni–Z	90.45(7)	90.06(7)	90.04(6)	90.28(6)	89.97(6)	89.98(6)	90.92(7)	92.93(10)	95.95(10)	87.83(9)	88.76(9)	87.76(10)	87.96(8)	96.32(4)	96.54(5)	76.96(7)	77.04(7)
Y–Ni–Z	171.30(7)	167.66(7)	169.86(6)	169.76(6)	170.43(6)	170.46(6)	161.02(6)	166.48(9)	164.46(9)	169.69(6)	171.02(7)	170.29(5)	170.65(6)	176.55(5)	177.20(5)	177.71(7)	177.15(7)
Octahedral distortion factor[a]																	
σ_{oct}	6.1		5.5		4.8		9.6	7.6		5.1		5.0		5.8		7.7	
Angle/° between the two Y1–N4–Z8 planes																	
α	89.19(11)		88.35(11)		89.10(9)		89.21(11)	87.47(16)		88.23(13)		87.52(13)		88.02(8)		89.03(9)	
Angle/° between the Y1–C2–C3–N4–Ni and N4–C5–C6–C7–Z8–Ni least squares planes																	
β	9.48(9)	9.02(8)	8.14(8)	11.14(8)	6.90(7)	6.92(7)	21.95(8)	7.85(12)	16.50(12)	27.52(10)	23.01(10)	26.29(8)	24.86(12)	5.24(6)	10.33(7)	3.6(2)	8.4(2)
Angle/° between the Y1–N4–Z8 plane and the N4–C5–C6–C7–Z8 least squares plane																	
	9.21(11)	14.69(11)	12.32(11)	16.46(11)	10.57(9)	10.48(9)	26.59(11)	8.12(16)	19.95(16)	36.93(13)	31.08(14)	36.24(12)	32.26(16)	13.83(8)	1.39(8)	1.69(12)	9.12(13)
Angle/° between the Y1–N4–Z8 plane and the Y1–C2–C3–N4 least squares plane																	
δ	4.52(13)	3.49(14)	2.63(13)	1.33(12)	1.40(11)	1.59(11)	21.17(13)	6.60(19)	13.27(19)	23.25(14)	21.25(15)	20.92(12)	24.29(18)	8.85(11)	7.87(10)	6.1(3)	12.3(3)

[a] The bond angle variance, σ_{oct},[18] is the average difference of the twelve *cis*-angles from the idealised value of 90° as shown in eqn (3). [b] This complex has two crystallographically independent molecules per asymmetric unit. [c] The two ligands in [(**L9**)$_2$Ni] are related by a crystallographic C_2 axis through the Ni atom.

Distortion of the ligands from planarity will adversely affect conjugation and decrease the stability of their nickel complexes. Planarity can be compared using the angle, β, between the least squares planes of the 5-membered (Ni–Y1–C2–C3–N4) and 6-membered (Ni–N4–C5–C6–C7–Z8) chelate rings. The complexes of **L2H**, **L3H** and **L22H**, which contain iminoquinoline units, have the most nearly flat *mer*-planes with β values between 5.24 and 11.14°. In Table 3 the angle γ, between the least squares plane of N4–C5–C6–C7–Z8 and the plane of the three donor atoms, measures the deviation of the phenolic/thiopyrazolone moiety from the donor plane and δ is the angle between the least squares planes of the imine moiety, Y1–C2–C3–N4, and the donor atoms, Y1–N4–Z8.

Deviation from regular octahedral geometry will also result from variation of the donor atoms Y and Z. The thioether (Y1 = S) bonds to nickel are longer (2.41–2.49 Å) than those from the quinoline (Y1 = N) and methoxy (Y1 = O) groups (2.08–2.14 and 2.17–2.21 Å respectively), leading to [(**L13**)$_2$Ni] and [(**L14**)$_2$Ni] having smaller bite angles in their 6-membered chelate rings (N4–Ni1–Z8 falls in the range 87.76–88.76°) than in the other salicylaldimine complexes. This forces the phenolic moiety to twist out of the plane of the donor atoms (γ is between 31.08 and 36.93°). There are no unusual features associated with the packing of the complexes in the solid state structures or with the inclusion of solvent molecules in the lattices. Further information is provided in the ESI.†

The crystal structures of the nickel(II) complexes provide information on the geometry around the nickel(II) cation and conformation of the ligands. Deviations from regular octahedral geometry, as determined by the bond angle variance (σoct)[18] according to eqn (3), and distortion of the ligands from a planar arrangement with the consequent loss of conjugation are expected to lower the stability of the complexes of the different extractants.

$$\sigma\text{oct} = \sum_{i=1}^{12}(\sigma_i - 90)^2 \qquad (3)$$

The quinoline-containing complexes [(**L2**)$_2$Ni], [(**L9**)$_2$Ni] and [(**L22**)$_2$Ni] have the most nearly planar ligands and the most nearly regular octahedral geometry around the nickel(II) centre as judged by the values listed in Table 3. On this basis the reagents containing this moiety and solubilising alkyl groups, **L4H**, **L5H** and **L20H**, may be expected to extractant nickel from more acidic solutions because they are likely to generate more stable complexes.

Solvent extraction studies

A strong extractant will displace the pH-dependent equilibrium in eqn (1) to favour the formation [L$_2$Ni], leading to nickel(II) extraction into the organic phase at a lower pH. Plots showing the pH-dependence of nickel(II) uptake from aqueous sulfate solutions by **L4H**, **L5H**, **L11H** and **L15H** into chloroform are presented in Fig. 8. No appreciable nickel extraction was detected below pH 2 and loading of the organic phase to a

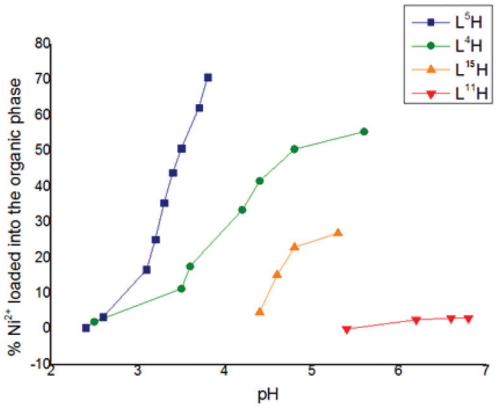

Fig. 8 The pH-dependence of nickel-loading by 0.005 M $CHCl_3$ solutions of **L4H**, **L5H**, **L11H** and **L15H** from an equal volume of aqueous 0.01 M $NiSO_4$. 100% loading is equivalent to that expected for formation of a 1 : 2 complex [Ni(L)$_2$].

theoretical nickel maximum value, assuming the 1 : 2 (metal : ligand) ratio in the extracted [L$_2$Ni] species, could not be achieved at pH ≥ 4.5 because nickel hydroxides were precipitated. **L15H** and **L11H** are too weak to obtain a value for $pH_{0.5}$ (the pH at which 50% of the theoretical loading is achieved), but it is possible to define the order of extractant strength as: **L5H** > **L4H** > **L15H** > **L11H**. **L5H** and **L4H** have identical N_2O^- donor sets but the incorporation of a nitro group *ortho* to the phenol oxygen atom in **L5H** increases the extractant strength by one pH unit based on $pH_{0.5}$ values, which correspond to approximately to an order of magnitude increase in the extraction distribution coefficient. The origin of this is discussed below. **L15H** and **L11H** also have nitro groups *ortho* to the phenol OH group but different Y donor atoms, a thioether and an ether. The NSO^- donor set of **L15H** can load nickel into the organic phase at a lower pH than **L11H**, which has a NO_2^- donor set, but both are significantly weaker than the quinoline containing reagents, **L4H** and **L5H**.

Imine extractants have low stability under acidic conditions and readily hydrolyse to form their component aldehydes and amines.[19] The low hydrolytic stability of the pyrazolone imine reagents **L20H–L22H** prohibited conventional studies of the pH dependence of metal-loading as in Fig. 8. Nevertheless, the binding preference for uptake of nickel(II) or iron(III) by the pyrazolone imine reagents could be investigated by mixing a toluene solution of preformed [(L)$_2$Ni] with aqueous $Fe_2(SO_4)_3$ (see Fig. 9). ICP-OES analysis of [(**L20**)$_2$Ni] solutions showed that nickel transferred to the aqueous phase and iron was taken up by the toluene solution. ^{13}C NMR analysis of the concentrated organic phase showed that extractant **L20H** had been hydrolysed to the parent acylpyrazolone. Formation of the charge neutral [(acypyrazolonate)$_3$Fe] complex is presumably favoured because the hard iron(III) ion is provided with an O_6^{3-} donor set. The thiopyrazolone complex [(**L22**)$_2$Ni] was stable under similar conditions and no iron was transported into the organic phase (Fig. 9). Soft sulfur donor atoms

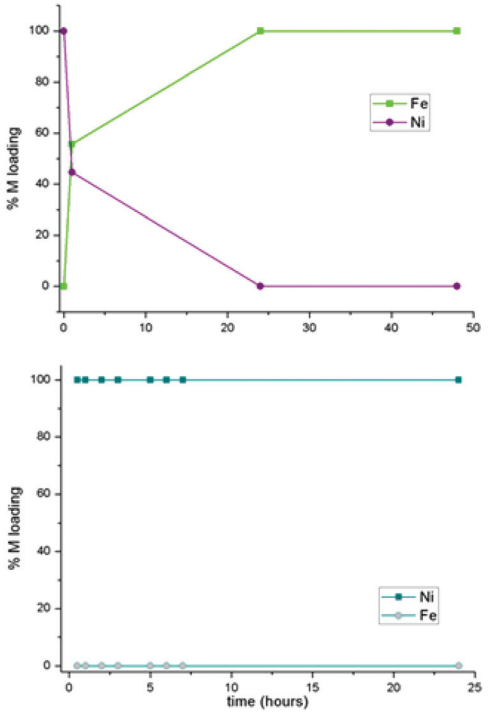

Fig. 9 Loading of nickel(II) and iron(III) when 1.8 mM solutions of [NiL_2] in toluene were contacted with a 1.8 mM aqueous solution of $Fe_2(SO_4)_3$ (**L20** top, **L22** bottom). The % metal loading is based on the ligand available in toluene forming [$Ni(L)_2$] or [$Fe(L_3)$] complexes.

provide a less favourable donor set for iron(III) and the formation of [$(L)_3Fe$] *via* hydrolysis of the imine can be assumed to be less thermodynamically favourable.

Computational studies

Previous work has shown that calculated (gas phase) enthalpies of formation, ΔE_f, for copper complexes formed by a series of phenolic oximes correlate with their measured strengths as solvent extractants.[20] The energies of the energy-minimised structures of the proligands **L6H**, **L7H**, **L16H–L19H**, the related ligands (L^-) and their complexes, [L_2Ni], were calculated (see ESI†) and used to evaluate the formation enthalpy (ΔE_f) associated with the process in eqn (4).

$$2LH + 2H_2O + Ni^{2+} \rightleftharpoons [(L)_2Ni] + 2H_3O^+ \quad (4)$$

To define the origins of the dependence of the variations of formation enthalpies on the nature of the proligands, the deprotonation enthalpies (ΔE_d) for the reaction in eqn (5) were calculated using eqn (6),

$$LH + H_2O \rightleftharpoons L^- + H_3O^+ \quad (5)$$

$$\Delta E_d = [L^-(E_{tot}) + H_3O^+(E_{tot})] - [LH(E_{tot}) + H_2O(E_{tot})] \quad (6)$$

and binding enthalpies (ΔE_b), the energy released in bringing together two preformed anions, L^-, and a Ni^{2+} cation in the gas phase were calculated using the terms in eqn (7);

$$\Delta E_b = [Ni_{complex}(E_{tot})] - [2L^-(E_{tot}) + Ni_{cation}(E_{tot})] + BSSE + 2RT \quad (7)$$

In eqn (6) and (7) E_{tot} is made up of the sum of the electronic (E_{el}), vibrational (E_{vib}), rotational (E_{rot}) and translational (E_{trans}) energies as shown in eqn (8).

$$E_{tot} = E_{el} + E_{vib} + E_{rot} + E_{trans} \quad (8)$$

The phenolic tautomer of **L6H** was shown to be 13 kJ mol^{-1} lower in energy than the quinone in the gas-phase, and a similar trend was established for the other salicylaldimines. The nickel(II) binding energies (ΔE_b) and proligand deprotonation energies (ΔE_d) were separately calculated, according to eqn (6) and (7), to determine how structural variations of the ligand affect these processes. An analysis of the energy terms in Table 4 provides an insight into the origins of the variations in formation energies of complexes in the gas phase which correlate with measured strengths of the extractant analogues (see below).

For the nitro-substituted ligands **L7H**, **L18H** and **L19H**, values of the calculated formation energies, ΔE_f, follow the trend of measured extractant strengths of the *t*-octyl homologues (see Fig. 8). Extractant strength varies with the nature of the donor set in the order $N_2O^- > NSO^- > NO_2^-$. The calculated deprotonation energy (ΔE_d) is more favourable for the nitro-substituted proligand, **L7H**, than for the unsubstituted analogue, **L6H**, by 61 kJ mol^{-1}. A similar trend was found for the other nitro-substituted proligands, **L18H** and **L19H**. Conversely, the nickel(II)-binding energies, ΔE_b, of the anionic forms of **L6H**, **L16H** and **L17H** are more favourable than their nitro-analogues (Table 4). This is consistent with the electron withdrawing nitro group increasing the acidity of the reagents whilst decreasing the basicity of their conjugate anions.

The low deprotonation energy of the thioether appears to arise from the sulfur not being able to form an effective intramolecular hydrogen bond with the phenolic hydrogen, making it easier for the latter to be released. The absence of an intramolecular thioether to phenolic hydrogen interaction is observed in the solid state structure of **L13H**, contrasting with the structure of the ether analogue **L9H** (molecule **b**) and the quinoline analogue **L2H**. Despite the thioether **L19H** having the lowest deprotonation energy, the formation energy of its nickel complex is much less favourable than that of the quinoline ana-

Table 4 Formation energies, ΔE_f, binding energies, ΔE_b, and deprotonation energies, ΔE_d, for proligands **L4H**, **L5H** and **L16–19H** calculated using B3LYP/6-31G(d,p)

Proligand	ΔE_f (kJ mol^{-1})	ΔE_d (kJ mol^{-1})	ΔE_b (kJ mol^{-1})
L6H (X = H and Y = N)	−1279	784	−3066
L16H (X = H and Y = O)	−1219	793	−3028
L17H (X = H and Y = S)	−1209	778	−2773
L7H (X = NO_2 and Y = N)	−1315	723	−2769
L18H (X = NO_2 and Y = O)	−1243	729	−2710
L19H (X = NO_2 and Y = S)	−1259	715	−2696

logue **L7H**. This arises because the binding energy of the conjugate anion to nickel(II) is much more favourable for the latter.

Conclusion

Despite being pre-organised by intramolecular hydrogen bonding to provide nearly orthogonal YNZ^- donor sets, the new tridentate reagents are not strong nickel(II) extractants. X-ray structure determination has shown that they form the expected 2 : 1 *mer*-complexes, but with significant deviations from regular octahedral geometry. Extraction strength is very dependent on the nature of the donor set, with N-donor quinoline reagents recovering nickel at a lower pH than their *o*-methoxyphenyl and *o*-thiomethoxyphenyl analogues. The introduction of electron-withdrawing substituents onto the chelating unit containing the ionisable proton increases extractant strength, *e.g.* the nickel(II)-extraction coefficient of the *o*-nitro-substituted reagent, **L5H**, is more than an order of magnitude greater than that of the unsubstituted analogue **L4H**.

The donor sets provided by the quinoline-containing reagents have slightly smaller angular distortions from regular octahedral geometry than those in the model complex [Ni(^{n}Pr–hydroxyoxime)$_2$(^{i}Pr–CO$_2$)$_2$], but the bond lengths to nickel(II) fall in a slightly wider range. If the regularity of the coordination geometry assumed by the nickel ion is an important criterion in defining the stability of complexes, favouring their formation in the extraction equilibrium, there are no obvious benefits provided by the new tridentate salicylaldimine reagents. The energies of formation of the nickel complexes in the gas phase, ΔE_f, evaluated by DFT calculations, show a good correlation with the measured $pH_{0.5}$ of the extractant analogues, providing further evidence that this modelling strategy is an effective tool for predicting the strength of cation exchange extractants and assessing the different effects of varying a substituent in a series of analogous compounds.

Because the calculations do not attempt to take account of solvation energies, the correlation between the energies of gas phase equilibria and those of equilibria involving two solvents is at first sight surprising, but this has now been observed in several different systems.[16,21,22] An important feature of each of these systems is that the only variable is the nature of a small substituent in a given class of extractant. The metal species removed from the aqueous phase and consequently the energy involved in hydration and dehydration of this and charge-balancing protons remain constant in a system. The small variations to substituents in the hydrophobic extractants are expected to result in minor differences in the solvation energies of complexed and uncomplexed forms of the extractants in the water-immiscible solvent. Consequently, the effects of substituents on both the ease of deprotonation of the extractant and the binding energy of the resulting anion to nickel(II) will make the major contribution to the relative strengths of a coherent series of extractants such as **L4H**, **L5H**, **L11H**, and **L15H**.

The strongest of the new extractants, the quinoline-containing reagents, would be able to operate under comparable conditions to synergistic mixtures of Versatic® 10 and α-hydroxyoximes, *i.e.* at pH > 3, after iron(III) has been precipitated as in the Goro and Bulong processes.[5,23] However, the currently tested versions do not have very high solubility in hydrocarbon solvents which will limit mass-transport efficiency. Imine linkages are susceptible to hydrolysis and consequently they would decompose in continuous operations under conditions similar to those used for Ni-recovery by Versatic 10/LIX 63 mixtures.[5]

Acknowledgements

We thank the EPSRC, Anglo American and Cytec Industries for funding PhD studentships for JWR and JRT and EaStCHEM for access to the Research Computing Facility.

Notes and references

1 D. J. Hanson, *Chem. Eng. News*, 2003, **81**, 82.
2 C. Biley, M. Pelser, P. den Hoed and M. Hove, *Proceedings of the 7th Southern African Base Metals Conference*, Mpumalanga, South Africa, 2013.
3 G. M. Mudd, *Ore Geol. Rev.*, 2010, **38**, 9–26.
4 R. G. McDonald and B. I. Whittington, *Hydrometallurgy*, 2008, **91**, 35–55.
5 S. Donegan, *Miner. Eng.*, 2006, **19**, 1234–1245.
6 J. T. Smit, J. D. T. Steyl and M. Pelser, *WO Pat.*, WO2011015991, 2011.
7 C. Bourget, B. Jakovljevic and D. Nucciarone, *Hydrometallurgy*, 2005, **77**, 203–218.
8 K. C. Sole and J. B. Hiskey, *Hydrometallurgy*, 1992, **30**, 345–365.
9 K. G. Fisher, *Proceedings of the Southern African Base Metals Conference 2011*, Phalaborwa, South Africa, 2011.
10 J. S. Preston, *Hydrometallurgy*, 1985, **14**, 171–188.
11 M. Tanaka, N. Nakasuka and S. Sasane, *J. Inorg. Nucl. Chem.*, 1969, **31**, 2591–2597.
12 C. Cheng, K. R. Barnard, W. Zhang and D. J. Robinson, *Solvent Extr. Ion Exch.*, 2011, **29**, 719–754.
13 K. R. Barnard, G. L. Nealon, M. I. Ogden and B. W. Skelton, *Solvent Extr. Ion Exch.*, 2010, **28**, 778–792.
14 K. R. Barnard and N. L. Turner, *Hydrometallurgy*, 2011, **109**, 29–36.
15 A. L. Nivorozhkin, A. I. Uraev, G. I. Bondarenko, A. S. Antsyshkina, V. P. Kurbatov, A. D. Garnovskii, C. I. Turta and N. D. Brashoveanu, *Chem. Commun.*, 1997, 1711–1712.
16 R. S. Forgan, B. D. Roach, P. A. Wood, F. J. White, J. Campbell, D. K. Henderson, E. Kamenetzky, F. E. McAllister, S. Parsons, E. Pidcock, P. Richardson, R. M. Swart and P. A. Tasker, *Inorg. Chem.*, 2011, **50**, 4515–4522.
17 A. Smith, *PhD*, University of Edinburgh, 1999.
18 K. Robinson, G. V. Gibbs and P. H. Ribbe, *Science*, 1971, **172**, 567–570.

19 J. R. Turkington, *PhD*, University of Edinburgh, 2011.
20 R. S. Forgan, *Inorg. Chem.*, 2011, **50**, 4515–4522.
21 R. J. Ellis, J. Chartres, D. K. Henderson, R. Cabot, P. R. Richardson, F. J. White, M. Schroeder, J. R. Turkington, P. A. Tasker and K. C. Sole, *Chem. – Eur. J.*, 2012, **18**, 7715–7728.
22 M. R. Healy, V. A. Cocallia, E. D. Doidge, A. J. Fischmann, J. B. Love, C. A. Morrison, J. W. Roebuck, T. Sassi and P. A. Tasker, *Proceedings of the International Solvent Extraction Conference*, Würzburg, Germany, 2014.
23 I. O. Mihaylov, E. Krause, D. F. Colton, Y. Okita, J.-P. Duterque and J.-J. Perraud, *CIM Mag.*, 2000, 93; B. I. Whittington and D. Muir, *Miner. Process. Extr. Metall. Rev.*, 2000, **21**, 527–599; D. S. Flett, *Principles and practices of solvent extraction*, Marcel Dekker, New York, 2nd edn, 2004, pp. 760–762.